Materials Advances

ROYAL SOCIETY OF CHEMISTRY

PAPER

View Article Online
View Journal | View Issue



Cite this: *Mater. Adv.*, 2025, 6, 9696

# Controlling emissive behaviour through molecular design: 2,3-bis(2,5-dimethylthiophen-3-yl)quinoxalines with variable fluorene substitution

Liudmila Loghina, *[a] Jiri Jancalek, [a] Jakub Houdek,[a] Zuzana Zmrhalova,[a] Roman Jambor [b] and Miroslav Vlcek [ab]

Received 8th October 2025,
Accepted 30th October 2025

DOI: 10.1039/d5ma01158b

rsc.li/materials-advances

We report a new family of donor–acceptor–donor (D–A–D) chromophores based on 2,3-bis(2,5-dimethyl thiophen-3-yl)quinoxaline, where the electronic and steric environment is tuned through fluorene substituents at the 5,8-positions. Variation of the 9,9-substituents (aryl, branched alkyl, and spiro-linked groups) enables systematic modulation of solubility, conformational rigidity, and intermolecular interactions while preserving the electron-deficient quinoxaline core. All synthesized derivatives (**DMTQ1–DMTQ5**) exhibit characteristic π–π* absorption around 380 nm and broad intramolecular charge-transfer (ICT) emission in solution (490–502 nm) with photoluminescence quantum yields up to 45% and lifetimes of 2.7–4.0 ns. A detailed solvatochromic and time-resolved study of DMTQ5 confirmed strong ICT character, manifested by red-shifted emission and polarity-dependent lifetime shortening. Electrochemical studies reveal consistent oxidation onsets (0.54–0.64 V *vs.* $Fc/Fc^+$), corresponding to HOMO levels of −5.34 to −5.44 eV, while LUMO energies (−2.57 to −2.67 eV) were derived from optical gaps of ∼2.8 eV. In the solid state, spin-coated films of selected derivatives exhibit pronounced photochromic switching of emission colour and intensity, a behaviour absent in solution and directly demonstrated using UV-LED excitation. These results establish fluorene substitution as a versatile strategy to direct emissive behaviour in quinoxaline-based chromophores, highlighting their potential as polarity-sensitive probes, light-responsive coatings, and optoelectronic materials.



## Introduction

Organic π-conjugated systems with donor–acceptor–donor (D–A–D) architectures offer a versatile platform for tuning optoelectronic properties, making them highly attractive for applications in organic light-emitting diodes (OLEDs), sensors, and photovoltaics.[1–6] Among various electron-deficient heteroaromatic cores, quinoxalines stand out due to their rigid planar structure, strong electron-accepting nature, and synthetic accessibility. Substitution at the 2,3-positions with electron-rich aryl groups, especially thiophenes, has proven particularly effective in promoting intramolecular charge transfer (ICT) and modulating photophysical behaviour. Recent advances have explored diverse substitution patterns on the quinoxaline core to tailor optical and electronic properties. In particular, varying the steric and electronic configuration of fluorene units at the 5,8-positions (*e.g.*, 9,9-diphenyl, spiro, branched alkyl) provides a modular handle to adjust planarity, extend conjugation, and control packing in the solid state, with direct consequences for spectral response and photoluminescence quantum yield (PL QY). Sigl *et al.* reported a fluorene–quinoxaline copolymer with high photoluminescence quantum yield and solid-state emissive behaviour.[7] They demonstrated that fluorene incorporation improves photostability and colour purity in OLED-relevant materials. Similarly, a planar alkylidene–fluorene–quinoxaline polymer (PAFDQ) demonstrates enhanced intramolecular charge transfer, compact packing, and favourable morphological properties.[8] Earlier work on quinoxaline-containing polyfluorenes with 2,3-bis(phenylene) substitution further supports the utility of such architectures in tailoring optoelectronic behaviour.

While various thiophene–quinoxaline frameworks have been reported, systematic studies on the effect of fluorene substitution, especially at the 9-position, remain limited. Several representative studies highlight the potential of quinoxaline-based materials in optoelectronics. Zhuang *et al.* developed D–A polymers that combine thiophene and quinoxaline motifs, exhibiting tunable optical band gaps through heteroatom variation.[9] Their computational and experimental studies demonstrated how the nature of the donor and the acceptor

[a] *Center of Materials and Nanotechnologies, Faculty of Chemical Technology, University of Pardubice, 530 02 Pardubice, Czech Republic. E-mail: liudmila.loghina@upce.cz*
[b] *Department of General and Inorganic Chemistry, Faculty of Chemical Technology, University of Pardubice, 532 10 Pardubice, Czech Republic*

influences the HOMO–LUMO energy levels and absorption profiles. Li *et al.* synthesized donor–acceptor copolymers containing carbazole and thieno[3,2-*b*]quinoxaline units (TTQx-based conjugated polymers) exhibiting broad absorption and PCEs up to 5% in organic photovoltaics.[10] The authors highlighted the role of extended π-conjugation in enhancing charge separation and light harvesting efficiency. Li *et al.* designed TADF quinoxaline emitters for OLEDs, achieving excellent efficiency and low singlet–triplet energy splitting $\Delta E_{ST}$.[11] The combination of rigid quinoxaline acceptors with twisted donors enabled efficient reverse intersystem crossing and delayed fluorescence. Yu *et al.* combined aggregation-induced emission (AIE) and TADF in fluorinated quinoxalines with an external quantum efficiency up to 23.5%.[12] Their work illustrates how fluorination and molecular rigidity synergistically promote bright emission in the solid state. Kim *et al.* demonstrated quinoxaline-based donor–acceptor polymers for solar cells with PCEs around 3.9%.[13] They emphasized the importance of backbone planarity and energy level alignment in optimizing device performance. Zhao *et al.* explored electrochromic quinoxaline polymers with high coloration efficiency and reversible switching.[14] The study linked the electrochromic response to π-electron delocalization, controlled by substitution patterns. Zhang *et al.* reported narrow-bandgap TTQx derivatives for high-contrast photonic materials.[15] Their materials exhibited strong intramolecular charge transfer and tunable emission across the visible to near-IR region. Despite significant progress in quinoxaline-based donor–acceptor systems, the development of structurally diverse chromophores with predictable emission behaviour remains challenging.

Herein, we present a new family of D–A–D-type chromophores based on 2,3-bis(2,5-dimethylthiophen-3-yl)quinoxaline, in which the donor strength and steric profile are systematically tuned by fluorene units introduced at the 5,8-positions. The choice of 2,5-dimethylthiophenes as donors was motivated by their strong electron-donating ability and the presence of methyl substituents, which improve solubility while restricting rotation and enhancing conformational stability. In parallel, fluorene derivatives bearing diverse 9,9-substituents (aryl, branched alkyl, and spiro-linked groups) were selected to probe how steric bulk, conformational flexibility, and electronic character influence the photophysical response. To our knowledge, this represents the first systematic investigation of quinoxaline chromophores that simultaneously combine electron-rich 2,5-dimethylthiophene donors with variably substituted fluorene groups at the 5,8-positions. This dual design enables fine control over emission colour and quantum yield by balancing π-extension, steric modulation, and substitution pattern. Beyond solution-state photophysics, we extend our analysis to spin-coated films, revealing a previously unexplored link between peripheral fluorene substitution and film-state photochromism. Through a comparative study of five derivatives (**DMTQ1–DMTQ5**), we establish clear structure–property relationships across solution and thin films, integrating solvatochromism, time-resolved photoluminescence, and cyclic voltammetry with a demonstration of reversible photochromic switching in films, including visualization under UV-LED excitation. This combined molecular and device-relevant perspective highlights fluorene substitution as a versatile handle to direct emissive behaviour in quinoxaline-based chromophores.

# Experimental

## Materials and methods

All reagents and solvents were obtained from commercial suppliers and used as received unless otherwise noted. Thionyl chloride, $NaBH_4$, $AlCl_3$, oxalyl dichloride, and *n*-BuLi solution (2.5 M in hexane) were purchased from Merck and TCI. $K_2CO_3$, 48% aqueous HBr, NaOH, and solvents were delivered from Penta. Appropriate alkyl bromides used in the synthesis of the intermediate compounds, 2-isopropoxy-4,4,5,5-tetramethyl-1,3,2-dioxaborolane, 2-bromo-9*H*-fluorene, 2,5-dimethylthiophene, tetrakis(triphenylphosphine)palladium(0), and *o*-phenylenediamine, were purchased from BLDpharm. All syntheses were performed under an Ar atmosphere using standard Schlenk techniques. Reactions were monitored by thin-layer chromatography (TLC) on silica gel 60 F254 plates. Column chromatography was carried out using silica gel (60 Å, 70–230 mesh). All products were dried under reduced pressure and stored in a dark environment.

## Synthetic procedures

**Synthesis of 5,8-dibromo-2,3-bis(2,5-dimethylthiophen-3-yl)quinoxaline 3.** A mixture of compound **1** (1.76 g, 0.0063 mol) and compound **2** (1.6 g, 0.006 mol) in 80 ml of absolute ethanol was stirred, and 10 ml of glacial acetic acid was added. The reaction mixture was refluxed for 5 h, then cooled to room temperature. The precipitated solid was filtered, washed with a small amount of cold ethanol, and air-dried. The resulting product was confirmed to be analytically pure and was used in subsequent reactions without further purification. Anal. calcd for $C_{20}H_{16}Br_2N_2S_2$ ($M_r$ = 508.29): C, 47.26; H, 3.17; Br, 31.44; N, 5.51; S, 12.61%. Found: C, 44.7; H, 3.21; Br, 30.90; N, 5.27; S, 12.58%. $^1$H NMR (500.13 MHz, $CDCl_3$), $\delta$: 6.84 (s, 2H), 6.53 (s, 2H), 2.46 (s, 6H), 2.39 (s, 6H). $^{13}$C NMR (125.76 MHz, $CDCl_3$), $\delta$: 151.02; 139.70; 138.81; 135.40; 134.45; 132.57; 127.00; 123.49; 15.09; 14.53. IR (ATR, $cm^{-1}$) 2911 (C–$H_{aliph}$), 1648 (C=$N_{quinoxaline}$), 1543 (C=$C_{thiophene}$), 1450 (C–$C_{arom}$), 1209 (C–C/C–S), 1142 (C–N), 969, 905 (C–H), 812 (thiophene ring deformation), 589 (C–Br).

**Synthesis of 2,3-bis(2,5-dimethylthiophen-3-yl)-5,8-bis(9,9-diphenyl-9*H*-fluoren-2-yl)quinoxaline (DMTQ1).** To a solution of compounds **3** (0.51 g, 0.001 mol) and **4a** (0.98 g, 0.0022 mol) in a mixture of 20 ml toluene and 10 ml ethanol, 2 M aqueous $K_2CO_3$ (0.91 g in 3.3 ml of distilled water) was added. The reaction mixture was degassed under stirring by evacuation and backfilling with argon. Tetrakis(triphenylphosphine)palladium(0) (0.13 g, 0.00011 mol) was then added, followed by a second degassing cycle. The resulting mixture was refluxed under an argon atmosphere for 6 hours until complete conversion was achieved. The reaction was cooled to room temperature and diluted threefold with diethyl ether. The precipitated crystals were collected by filtration, washed with water and ether directly on the filter, and

air-dried to give an orange powder. The crude product was purified by flash chromatography on silica gel (petroleum ether : $CH_2Cl_2$ = 10 : 3.5), affording the pure compound. Yellow powder; yield: 0.92 g (94%). Anal. calcd for $C_{70}H_{50}N_2S_2$ ($M_r$ = 983.30): C, 85.50; H, 5.13; N, 2.85; S, 6.52. Found: C, 83.35%; H, 5.01%; N, 2.52%; S, 5.96. $^1$H NMR (500.13 MHz, $CDCl_3$), $\delta$: 7.86–7.79 (m, 3H), 7.75 (s, 1H), 7.70 (s, 1H), 7.43–7.42 (d, $^3J_{H,H}$ = 7.67 Hz, 1H), 7.36 (t, $^3J_{H,H}$ = 7.24 Hz, 1H), 7.28–7.25 (m, 5H), 7.16–7.15 (m, 6H), 6.33 (s, 1H), 2.29 (s, 3H), 2.09 (s, 3H). $^{13}$C NMR (125.76 MHz, $CDCl_3$), $\delta$: 151.52; 150.79; 149.21; 145.96; 140.01; 139.78; 139.44; 138.64; 138.27; 137.76; 135.66; 134.70; 130.87; 129.75; 128.20; 127.65; 127.49; 127.09; 126.59; 126.27; 120.26; 119.33; 65.63; 15.09; 14.08. IR (ATR, $cm^{-1}$) 3054 (C–$H_{arom}$), 2911 (C–$H_{aliph}$), 1648 (C=$N_{quinoxaline}$), 1446 (C–$C_{arom}$/$CH_3$ bending), 1214 (C–C/C–S), 825, 728, 690 (C–$H_{arom}$ out-of-plane/phenyl bending).

**Synthesis of 5,8-di(9,9′-spirobi[fluoren]-2-yl)-2,3-bis(2,5-dimethyl thiophen-3-yl)quinoxaline (DMTQ2).** Compound **DMTQ2** was synthesized following the same procedure as **DMTQ1**, employing intermediates **3** and **4b**. Yellow powder; yield: 83%. Anal. calcd for $C_{70}H_{46}N_2S_2$ ($M_r$ = 979.27): C, 85.86; H, 4.73; N, 2.86; S, 6.55. Found: C, 83.57%; H, 4.60%; N, 2.62%; S, 5.62. $^1$H NMR (500.13 MHz, $CDCl_3$), $\delta$: 7.85–7.84 (d, $^3J_{H,H}$ = 8.00 Hz, 1H), 7.82–7.80 (d, $^3J_{H,H}$ = 7.63 Hz, 1H), 7.75–7.73 (d, $^3J_{H,H}$ = 7.63 Hz, 2H), 7.70–7.68 (dd, $^3J_{H,H}$ = 7.50 Hz, $^4J_{H,H}$ = 1.35 Hz, 1H), 7.42 (s, 1H), 7.32–7.26 (m, 3H), 7.20 (s, 1H), 7.05–7.01 (m, 3H), 6.93 (d, $^4J_{H,H}$ = 0.98 Hz, 1H), 6.74–6.73 (d, $^3J_{H,H}$ = 7.51 Hz, 2H), 6.65–6.63 (d, $^3J_{H,H}$ = 7.63 Hz, 1H), 6.13 (d, $^4J_{H,H}$ = 0.61 Hz, 1H), 2.22 (s, 3H), 1.89 (s, 3H). $^{13}$C NMR (125.76 MHz, $CDCl_3$), $\delta$: 149.32; 148.85; 148.67; 148.14; 141.65; 141.42; 141.08; 139.44; 138.44; 138.20; 137.92; 135.38; 134.39; 131.02; 129.59; 127.80; 127.68; 127.60; 126.78; 125.95; 124.25; 123.85; 119.98; 119.81; 119.16; 66.02; 29.64; 14.99; 13.86. IR (ATR, $cm^{-1}$) 3063 (C–$H_{arom}$), 2911 (C–$H_{aliph}$), 1644 (C=$N_{quinoxaline}$), 1441 ($CH_3$/C–$C_{arom}$), 1137 (C–C/C–S), 830, 728 (C–$H_{arom}$), 635 (ring deformation/skeletal vibration).

**Synthesis of 5,8-bis(9,9-didecyl-9*H*-fluoren-2-yl)-2,3-bis(2,5-dimethylthiophen-3-yl)quinoxaline (DMTQ3).** Product **DMTQ3** was synthesized following the same procedure as **DMTQ1**, employing intermediates **3** and **4c**. The product was isolated by extraction from the reaction mixture with dichloromethane, followed by purification on silica gel (PE : $CH_2Cl_2$ = 1 : 0.35). Orange oil; yield: 87%. Anal. calcd for $C_{86}H_{114}N_2S_2$ ($M_r$ = 1239.99): C, 83.30; H, 9.27; N, 2.26; S, 5.17. Found: C, 82.03%; H, 8.74%; N, 2.18%; S, 5.26%. $^1$H NMR (500.13 MHz, $CDCl_3$), $\delta$: 7.87 (s, 1H), 7.77–7.71 (m, 4H), 7.34–7.27 (m, 3H), 6.43 (s, 1H), 2.30 (s, 3H), 2.16 (s, 3H), 1.96 (t, $^3J_{H,H}$ = 8.14 Hz, 4H), 1.20–1.00 (m, 28H), 0.79 (t, $^3J_{H,H}$ = 7.10 Hz, 6H), 0.75–0.71 (m, 2H), 0.67–0.63 (m, 2H). $^{13}$C NMR (125.76 MHz, $CDCl_3$), $\delta$: 151.09; 150.35; 148.89; 140.94; 140.25; 139.91; 138.69; 137.75; 137.57; 135.70; 134.62; 130.07; 129.68; 127.07; 126.86; 126.68; 124.97; 122.91; 119.71; 118.83; 55.09; 40.30; 31.82; 30.06; 29.56; 29.48; 29.28; 29.22; 23.88; 22.60; 15.09; 14.25; 14.05. IR (ATR, $cm^{-1}$) 2919, 2851 (C–$H_{aliph}$), 1610 (C=$N_{quinoxaline}$), 1446 ($CH_2$/$CH_3$), 1142 (C–C/C–S), 825, 737 (C–$H_{arom}$).

**Synthesis of 5,8-bis(9,9-bis(2-ethylhexyl)-9*H*-fluoren-2-yl)-2,3-bis(2,5-dimethylthiophen-3-yl)quinoxaline (DMTQ4).** Product **DMTQ4** was synthesized following the same procedure as **DMTQ1**, employing intermediates **3** and **4d**. The product was isolated by extraction from the reaction mixture with dichloromethane, followed by purification on silica gel (PE : $CH_2Cl_2$ = 1 : 0.35). Orange semisolid; yield: 71%. Anal. calcd for $C_{78}H_{98}N_2S_2$ ($M_r$ = 1127.78): C, 83.07; H, 8.76; N, 2.48; S, 5.69. Found: C, 82.46%; H, 9.32%; N, 1.99%; S, 4.76. $^1$H NMR (500.13 MHz, $CDCl_3$), $\delta$: 7.91–7.87 (m, 2H), 7.82–7.78 (m, 3H), 7.45–7.43 (dd, $^3J_{H,H}$ = 7.45 Hz, $^4J_{H,H}$ = 2.41 Hz, 1H), 7.38 (t, $^3J_{H,H}$ = 7.45 Hz, 1H), 7.31 (t, $^3J_{H,H}$ = 7.45 Hz, 1H), 6.50–6.47 (d, $^3J_{H,H}$ = 13.90 Hz, 1H), 2.37–2.36 (d, $^4J_{H,H}$ = 2.73 Hz, 3H), 2.24 (d, $^4J_{H,H}$ = 2.43 Hz, 3H), 2.12–2.03 (m, 4H), 0.78–0.72 (m, 17H), 0.68–0.63 (m, 2H), 0.59–0.56 (m, 9H), 0.53–0.49 (m, 2H). $^{13}$C NMR (125.76 MHz, $CDCl_3$), $\delta$: 140.17; 140.06; 138.81; 138.75; 137.79; 137.74; 137.58; 137.53; 137.22; 137.20; 137.16; 135.88; 135.81; 134.45; 134.41; 134.38; 130.53; 130.51; 129.34; 129.31; 127.37; 127.29; 126.73; 126.34; 125.92; 125.80; 125.77; 124.11; 124.10; 119.70; 118.59; 54.98; 44.66; 34.71; 34.65; 33.82; 33.78; 28.30; 28.27; 28.17; 27.00; 22.77; 22.72; 15.15; 15.13; 14.37; 14.35; 14.07; 13.92; 10.35. IR (ATR, $cm^{-1}$) 2914, 2856 (C–$H_{aliph}$), 1610 (C=$N_{quinoxaline}$), 1446 ($CH_2$/$CH_3$), 1142 (C–C/C–S), 825, 741 (C–$H_{arom}$).

**Synthesis of 5,8-bis(9,9-diisobutyl-9*H*-fluoren-2-yl)-2,3-bis(2,5-dimethylthiophen-3-yl)quinoxaline (DMTQ5).** Compound **DMTQ5** was synthesized following the same procedure as **DMTQ1**, employing intermediates **3** and **4e**. The product was isolated by extraction from the reaction mixture with dichloromethane, followed by purification on silica gel (PE : $CH_2Cl_2$ = 1 : 0.35). Yellow semisolid; yield: 68%. Anal. calcd for $C6_2H_{66}N_2S_2$ ($M_r$ = 903.34): C, 82.44; H, 7.36; N, 3.10; S, 7.10. Found: C, 81.56%; H, 7.54%; N, 2.83%; S, 6.43%. $^1$H NMR (500.13 MHz, $CDCl_3$), $\delta$: 7.84 (s, 1H), 7.78–7.71 (m, 4H), 7.36–7.34 (d, $^3J_{H,H}$ = 7.43 Hz, 1H), 7.33–7.30 (td, $^3J_{H,H}$ = 7.43 Hz, $^4J_{H,H}$ = 0.87 Hz, 1H), 7.21–7.24 (td, $^3J_{H,H}$ = 7.43 Hz, $^4J_{H,H}$ = 0.80 Hz, 1H), 6.39 (d, $^4J_{H,H}$ = 0.80 Hz, 1H), 2.29 (s, 3H), 2.10 (s, 3H), 1.97–1.96 (m, 4H), 0.95–0.87 (m, 2H), 0.37–0.33 (dd, $^3J_{H,H}$ = 6.71 Hz, $^3J_{H,H}$ = 11.03 Hz, 12H). $^{13}$C NMR (125.76 MHz, $CDCl_3$), $\delta$: 150.94; 150.11; 149.08; 141.14; 140.33; 140.12; 138.85; 137.64; 137.36; 135.68; 134.46; 130.07; 129.55; 127.15; 126.71; 126.58; 125.86; 123.65; 119.78; 118.86; 54.83; 50.31; 24.57; 24.56; 24.44; 15.08; 14.11. IR (ATR, $cm^{-1}$) 2953, 2906 (C–$H_{aliph}$), 1606 (C=$N_{quinoxaline}$), 1446 ($CH_3$/$CH_2$), 1142 (C–C/C–S), 830, 737 (C–$H_{arom}$).

## Results and discussion

### Synthesis and molecular design

The synthetic approach employed in this study enables the modular construction of a new family of donor–acceptor–donor (D–A–D) chromophores based on the 2,3-bis(2,5-dimethylthio phen-3-yl)quinoxaline core, decorated with variably substituted fluorene units at the 5,8-positions (Scheme 1). The design rationale centres on controlling the emissive behaviour *via* systematic modification of both donor strength and steric/electronic environment at the periphery.

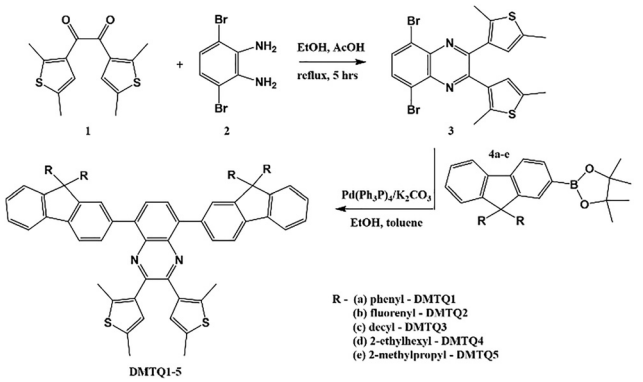


Scheme 1 Preparation of **DMTQ** chromophores bearing variable fluorene substituents.

Detailed experimental procedures and complete characterization data for all intermediates and final compounds are available in the SI.[16–21] As outlined in Scheme 1, the route begins with the condensation of intermediates **1** and **2** in refluxing ethanol and acetic acid affords the dibromoquinoxaline core **3**.[19]

New structures **DMTQ1–DMTQ5** were synthesized *via* Suzuki–Miyaura cross-coupling[22] between the corresponding boronic ester **4a–e**[23,24] and 5,8-dibromo-2,3-bis(2,5-dimethylthiophen-3-yl)quinoxaline **3**. This modular approach enables efficient diversification at the 5,8-positions of the quinoxaline scaffold, yielding chromophores with finely tunable optical and morphological properties.

All products share a central 2,3-bis(2,5-dimethylthiophen-3-yl)quinoxaline core, which ensures an extended D–A–D-type conjugation. Variation in the 9-substituents on the fluorene fragments allowed for systematic tuning of solubility, conformational dynamics, and solid-state behaviour: **DMTQ1** contains diphenyl-substituted fluorene units, which enhance π-conjugation while maintaining rigidity due to the restricted rotation of the aryl groups.[25] This configuration promotes efficient intramolecular charge transfer and high fluorescence quantum yields in solution. **DMTQ2** incorporates spirofluorene moieties, which are known to suppress π–π stacking in the solid state and improve morphological stability. The spiro architecture imparts three-dimensionality, reducing aggregation-induced quenching and enabling brighter thin-film emission. **DMTQ3** features long linear *n*-decyl chains at the 9-position of fluorene. These aliphatic substituents enhance solubility in nonpolar organic solvents and facilitate solution-processability, while introducing additional molecular flexibility. **DMTQ4** features branched 2-ethylhexyl groups, providing excellent solubilizing power and steric hindrance. This substitution aids in preventing dense packing in the solid state, thus preserving emissive behaviour in films. **DMTQ5** incorporates compact, branched 9,9-diisobutylfluorene fragments, which combine moderate bulk and flexibility. These substituents enable good solubility in both polar and non-polar media, making **DMTQ5** a suitable model for solvatochromic and film-based studies. This modular approach ensures that all five target compounds are accessible through the same synthetic sequence, offering a powerful framework for correlating structural variation with photophysical behaviour. To the best of our knowledge, all **DMTQ** derivatives, as well as intermediate **8**, represent novel compounds not previously reported in the literature.

## Structural characterization

All final compounds **DMTQ1–DMTQ5** were characterized by $^{1}$H and $^{13}C\{^{1}H\}$ NMR spectroscopy, confirming the successful formation of the conjugated quinoxaline–thiophene–fluorene framework. The $^{1}$H NMR spectra display characteristic singlets corresponding to the methyl groups on the thiophene rings ($\delta$ = 2.1–2.5 ppm) and aromatic resonances from both the quinoxaline core and the fluorene units ($\delta$ = 6.0–8.0 ppm). The central protons at positions 6 and 7 of the quinoxaline ring appear consistently as a singlet around $\delta$ = 6.3–6.5 ppm, confirming the symmetrical substitution at positions 2,3- and 5,8.[26] In compounds **DMTQ3–DMTQ5**, the presence of extended or branched alkyl chains leads to additional signals in the aliphatic region ($\delta$ = 0.5–2.0 ppm), including multiplets from methylene groups and terminal methyl triplets. For example, **DMTQ3** (didecyl-substituted) exhibits well-resolved aliphatic signals typical of long linear chains, while **DMTQ5** (diisobutyl) shows characteristic patterns for branched alkyl groups.[27] **DMTQ4** was synthesized using commercially available racemic 2-ethylhexyl bromide, resulting in a mixture of stereoisomers. This leads to signal doubling in both $^{1}$H and $^{13}C\{^{1}H\}$ NMR spectra, as a consequence of the diastereomeric environments around the chiral centres. The $^{13}C\{^{1}H\}$ NMR spectra are consistent with the proposed structures and exhibit clear signals from the quinoxaline and thiophene rings ($\delta \sim$ 135–150 ppm), methyl groups ($\delta \sim$ 14–15 ppm), and aliphatic carbons of the substituents ($\delta \sim$ 10–35 ppm). In **DMTQ1** and **DMTQ2**, the spectra are dominated by aromatic carbon signals from the diphenyl and spirobifluorene units, confirming their incorporation. All compounds exhibit high symmetry in solution, as indicated by the presence of single sets of methyl and thiophene proton signals, with no evidence of conformational isomerism or restricted rotation in $CDCl_3$. This suggests a relatively rigid and planar D–A–D architecture in solution. The spectral patterns also remain nearly invariant across the series in the conjugated core region, indicating that electronic communication is preserved regardless of peripheral fluorene substitution. Full $^{1}$H and $^{13}C\{^{1}H\}$ NMR spectra of all synthesized compounds are provided in the SI. In addition, elemental analysis and FTIR spectra support the assigned structures.

## Photophysical behaviour in solution

To evaluate the optical properties of the newly synthesized **DMTQ** chromophores and gain insight into their structure–property relationships, we investigated their absorption, excitation, and emission behaviour in solution. The five representative quinoxaline derivatives (**DMTQ1–DMTQ5**) were selected to illustrate the effect of 5,8-substitution on their photophysical characteristics, while maintaining a constant 2,3-substitution

pattern with electron-rich 2,5-dimethylthiophene units. All measurements were performed in chloroform, unless stated otherwise, using freshly prepared and optically dilute solutions. The compounds exhibit moderate solubility in $CHCl_3$ and other organic solvents, allowing for the accurate analysis of their concentration-dependent behaviour and solvent effects.

This section presents a comparative study of their UV-Vis absorption profiles, steady-state emission and excitation spectra, time-resolved fluorescence measurements, and solvatochromic response. These data are crucial for understanding how the molecular design, in particular the steric and electronic nature of the fluorene substituents, affects the photophysical performance in solution. The findings also provide a basis for selecting optimal candidates for solid-state and device-related studies presented in subsequent sections.

All five compounds (**DMTQ1–DMTQ5**) display qualitatively similar absorption profiles in chloroform, characterized by three main bands in the UV-Vis region (Fig. 1(a)). The lowest-energy transition, centred at 375–380 nm, remains virtually unchanged across the series, reflecting the dominant contribution of the common quinoxaline core to this π–π* transition. This band exhibits minimal sensitivity to substitution, consistent with a localized excitation on the central electron-deficient chromophore.[28] In contrast, the next absorption band (310–320 nm) demonstrates noticeable variations in both intensity and shape, which can be attributed to electronic and conformational differences introduced by the substituents at the 9-position of the fluorene units.[29] For example, **DMTQ2** (spirobifluorene) shows a broader and more structured band, whereas **DMTQ4** (bearing branched 2-ethylhexyl chains) exhibits a slightly hypsochromically shifted and less intense feature, indicating reduced conjugation and increased torsional disorder.[30]

The high-energy region (240–270 nm) reveals the most prominent differences. Each compound exhibits a distinct signature: **DMTQ1** shows a defined absorption band at 246 nm; **DMTQ2** displays a shoulder at 268 nm; **DMTQ3** presents a clear band at 254 nm; **DMTQ4** absorbs at 252 nm; and **DMTQ5** shows a weak shoulder near 256 nm (Table 1). These features likely originate from transitions localized on the peripheral aromatic units and are strongly affected by steric and electronic effects of the substituents. In the 240–270 nm range, the spectra comprise weak, substituent-localized transitions that are less apparent in normalized plots. **DMTQ5** demonstrates a broader composite envelope than **DMTQ4**, which we attribute to inhomogeneous broadening from compact diisobutyl-induced torsional microstates and the higher sensitivity of this high-energy region to specific solvation around different 9,9-substituents. These effects modulate the apparent width/intensity without implying aggregation or experimental artefacts. To evaluate the concentration-dependent absorption behaviour, UV-Vis spectra of **DMTQ2** were recorded in chloroform across the range of 0.0005–0.01 g $ml^{-1}$. As shown in Fig. 1(b), a proportional increase in absorbance is observed with rising concentration, and the overall shape of the spectrum remains consistent throughout

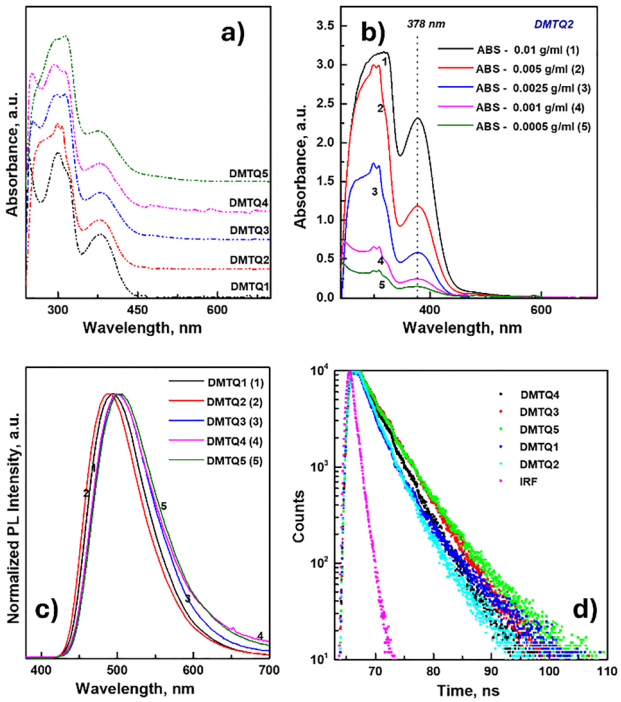


Fig. 1 Photophysical properties of **DMTQ** derivatives in solution. (a) UV-Vis absorption spectra of **DMTQ1–DMTQ5** (measured in $CHCl_3$, $c = 1 \times 10^{-5}$ M); (b) concentration-dependent absorption spectra of **DMTQ2** in $CHCl_3$ (0.01–0.0005 g $ml^{-1}$); (c) normalized photoluminescence (PL) spectra of **DMTQ1–DMTQ5** in $CHCl_3$ ($\lambda_{exc}$ = 375 nm, $c$ = 0.005 g $ml^{-1}$); (d) time-resolved PL decay profiles of **DMTQ1–DMTQ5** in $CHCl_3$ ($\lambda_{exc}$ = 375 nm, $\lambda_{em}$ = 505 nm).

the series, suggesting the absence of significant aggregation under the studied conditions. The main absorption band at ~378 nm increases linearly with concentration, indicating its origin in a well-defined π–π* transition of the conjugated backbone.[31] Notably, no new absorption bands, broadening, or bathochromic shifts are detected even at the highest concentrations, implying that **DMTQ2** retains its monomeric, non-aggregated state in solution. This phenomenon reflects its rigid and sterically demanding structure, which effectively suppresses intermolecular π–π interactions.[32] The normalized emission spectra of all five **DMTQ** derivatives in chloroform are presented in Fig. 1(c). Despite sharing the same quinoxaline–thiophene core, the five derivatives display only modest variations in solution-state emission. In $CHCl_3$, the maxima are 487–502 nm (Table 1), with **DMTQ2** being the most blue-shifted (487 nm), **DMTQ3–DMTQ5** essentially overlapping at 501–502 nm, and **DMTQ1** slightly blue-shifted relative to **DMTQ3–DMTQ5** (494 nm). The normalized spectra are broadly similar, showing only subtle differences in the long-wavelength tail (>580 nm). These small shifts are consistent with minor changes in electronic coupling and conformational freedom induced by the 9,9-substituents, while the common core dominates the lowest-energy transition.[33] These shifts can be rationalized by considering both the electronic and steric effects of the substituents at the 9,9-position of fluorene. Slight variations in donor strength and electron density distribution

Table 1 Optical and electrochemical parameters of **DMTQ1–DMTQ5**, including absorbance ($\lambda_{ABS}$)/excitation ($\lambda_{EXC}$)/emission ($\lambda_{PL}$) maxima, Stokes shifts, optical band gap ($E_g$), oxidation onset potential ($E_{onset}$), HOMO/LUMO energy levels, PL QY, and excited-state lifetimes ($\tau_{avr}$)

| | DMTQ1 | DMTQ2 | DMTQ3 | DMTQ4 | DMTQ5 |
|---|---|---|---|---|---|
| Absorbance maxima, $\lambda_{ABS}$, nm | 380 | 378 | 380 | 380 | 380 |
| Excitation maxima, $\lambda_{EXC}$, nm | 344 | 342 | 375 | 375 | 375 |
| Emission maxima, $\lambda_{PL}$, nm | 494 | 487 | 501 | 501 | 502 |
| Stokes shift, nm | 150 | 145 | 126 | 126 | 127 |
| Optical band gap, $E_g$, eV | 2.77 | 2.77 | 2.77 | 2.77 | 2.77 |
| Oxidation onset potential, $E_{onset}$, V | 0.55 | 0.64 | 0.59 | 0.54 | 0.60 |
| HOMO energy level, eV | 5.35 | 5.44 | 5.39 | 5.34 | 5.40 |
| LUMO energy level, eV | 2.58 | 2.67 | 2.62 | 2.57 | 2.63 |
| PL Quantum yield, PL QY, $\Phi$% | 40 | 38 | 45 | 37 | 38 |
| Fitting results of the PL decay curves, $\tau_{avr}$, ns | 2.97 | 2.72 | 3.79 | 3.26 | 3.95 |

The relative PL quantum yields (PL QY) of **DMTQ1–DMTQ5** were investigated at ambient conditions in $CHCl_3$, using quinine sulfate (0.01 M $H_2SO_4$, PL QY = 0.54) as a standard.[34]

modify the local HOMO level and influence the efficiency of intramolecular charge transfer within the quinoxaline–thiophene core. At the same time, the steric demand of the substituents determines the torsional freedom between the donor and acceptor units: bulkier and branched groups (*e.g.*, 2-ethylhexyl) restrict planarization and reduce effective conjugation, while more flexible or compact groups (such as *n*-decyl and diisobutyl) permit closer approach of the π-systems and enhanced coupling. These combined effects result in the subtle yet measurable differences observed in emission maxima and lifetimes across the **DMTQ1–DMTQ5** series. The influence of these factors becomes even more pronounced in the solid state, where molecular packing and conformational relaxation further amplify the differences in emissive behaviour.

Overall, this comparison demonstrates that subtle structural modifications at the fluorene periphery allow fine-tuning of emission properties while preserving the π-conjugated emission framework.

Fluorescence decay profiles of the five **DMTQ** derivatives in chloroform are presented in Fig. 4(d). All samples were excited at 375 nm, and emission was monitored at their respective maxima. The decay curves are well-fitted to a monoexponential function, indicating the presence of a single dominant emissive state that depends on the molecular structure.[35]

Among the five derivatives, **DMTQ5** exhibits the longest lifetime (~3.95 ns), consistent with its relatively high emission intensity and presumed reduced non-radiative relaxation. **DMTQ3** and **DMTQ4** exhibit intermediate lifetimes (~3.26–3.79 ns), whereas **DMTQ1** has a slightly shorter decay (~2.97 ns), which may be attributed to steric hindrance or rigidification effects impacting excited-state dynamics.[36] Notably, **DMTQ2** (spirobifluorene derivative) displays the shortest lifetime (~2.72 ns), in agreement with its comparatively lower photoluminescence quantum yield. Although **DMTQ2** and **DMTQ5** show nearly identical photoluminescence quantum yields in solution, their lifetimes differ because the rates of radiative and non-radiative decay are both faster in **DMTQ2**. The spirobifluorene groups in **DMTQ2** create a more rigid and sterically constrained geometry that enhances electronic coupling and increases the probability of photon emission, while simultaneously facilitating faster relaxation through vibrational pathways. As a result, the overall excited-state decay is quicker, giving a shorter lifetime while maintaining a similar quantum yield. In contrast, the more flexible diisobutyl substituents in **DMTQ5** slow down these processes, leading to a longer-lived emissive state. A more detailed comparison of the data summarized in Table 1 provides additional insight into the excited-state behaviour of the **DMTQ** series. The PL QYs ($\Phi$ = 37–45%) are relatively high for quinoxaline-based donor–acceptor–donor chromophores and indicate efficient radiative deactivation. The highest value was observed for **DMTQ3** (45%), consistent with its long lifetime (3.79 ns) and flexible, alkylated environment, which minimizes aggregation in solution. In contrast, the spirobifluorene derivative **DMTQ2** exhibits both the lowest lifetime (2.72 ns) and the lowest $\Phi$ among the series, which can be attributed to its more rigid and sterically hindered geometry, restricting conformational relaxation in the excited state. The gradual increase of lifetimes from **DMTQ1** to **DMTQ5** suggests that the substitution at the 9,9-position of fluorene affects not only electronic coupling but also the balance between radiative and nonradiative decay pathways. These results confirm that fluorene substitution not only affects the absorption and emission characteristics but also governs excited-state relaxation processes, providing a means to modulate fluorescence lifetime by structural design. Notably, while the absorption edge is dominated by the quinoxaline–thiophene core and remains nearly unchanged, variation of the 9,9-substituents on fluorene modulates solubility, conformational flexibility, and film packing, which directly affects $\Phi$ and $\tau$ as well as the solid-state/photochromic response, without significantly altering the core optical gap.

### Solvatochromic behaviour of DMTQ5

To prove the effect of solvent polarity on the emissive properties of the synthesized chromophores, **DMTQ5** was selected as a representative compound for a detailed solvatochromic study. This molecule was chosen due to its enhanced solubility in both polar and non-polar media, its structurally flexible, aliphatically substituted fluorene moieties, which are expected to promote conformational adaptability and stronger interactions with the solvent environment. Among the **DMTQ** series, **DMTQ5** combines a typical donor–acceptor–donor (D–A–D)

architecture with bulky 9,9-diisobutyl substituents, allowing it to effectively report on local polarity through changes in its photoluminescence response.[37]

The absorption spectra of compound **DMTQ5** were recorded in solvents of varying polarity to evaluate its solvatochromic response (Fig. 2(a)). These include non-polar (cyclohexane), moderately polar (chlorobenzene, chloroform, THF), and highly polar solvents (DMF, DMSO, methanol). The spectra consistently exhibit three major absorption features in the UV-Vis region, accompanied by solvent-specific shoulders or additional high-energy bands.[38] The main absorption band centred around 373–380 nm corresponds to a low-energy π–π* charge-transfer (CT) transition, most likely involving electron donation from the electron-rich 2,5-dimethylthiophene rings to the electron-deficient quinoxaline core. This band exhibits a subtle bathochromic shift with increasing solvent polarity – from 373 nm in methanol and 374 nm in cyclohexane to 380 nm in chloroform and 379 nm in chlorobenzene – indicating partial CT character of the transition. The relatively minor shift suggests a limited dipole moment changing between the ground and excited states. A second, moderately intense absorption feature appears around 309–315 nm in all solvents and remains nearly invariant with polarity. This band is assigned to a localized π–π* transition on the aromatic fluorene or thiophene moieties. The third, higher-energy transition (290–297 nm) exhibits slightly more variability between solvents and is generally weaker, sometimes appearing only as a shoulder (*e.g.*, in chlorobenzene, at ∼299 nm).

Solvent-specific features were also noted. A pronounced fourth absorption band or a clear shoulder in the 250–263 nm range emerges in several solvents: cyclohexane and chloroform exhibit well-defined shoulders at 259 nm; THF shows a shoulder at 252 nm; MeOH displays a more pronounced shoulder at 254 nm; DMSO and DMF reveal distinct high-energy absorption bands at 263 and 261 nm, respectively. Notably, the shoulder completely disappears in DMF, resulting in a sharp and intense new absorption band at 261 nm. This phenomenon is attributed to the high polarity and optical transparency of DMF, which may stabilize and enhance the oscillator strength of transitions that are otherwise weak or forbidden in less polar environments.[39] Overall, **DMTQ5** exhibits a moderate positive solvatochromism, with the CT band red-shifting slightly in more polar solvents.

The appearance or intensification of higher-energy bands (especially in DMF and DMSO) supports the presence of solvent-stabilized excited states and the resolution of hidden transitions. The persistence of the lower bands and the consistency of their spectral shapes imply a rigid, conjugated chromophore with only limited environmental sensitivity in its ground-state geometry.

The emission spectra of compound **DMTQ5** were recorded in the same series of solvents to assess its photoluminescent solvatochromic phenomenon. In contrast to the relatively modest shifts observed in absorption, the emission maxima demonstrate a pronounced bathochromic response to increasing solvent polarity (Fig. 2(b)). In non-polar cyclohexane, **DMTQ5** exhibits structured fluorescence with a maximum at 479 nm, while in highly polar methanol, the emission is significantly red-shifted to 523 nm – a total shift of 44 nm across the solvent series. This trend suggests that the emissive excited state possesses notable intramolecular charge-transfer (ICT) character, with electron density migrating from the peripheral 2,5-dimethylthiophene-fluorene segments toward the electron-deficient quinoxaline core upon photoexcitation.[40] The increasing stabilization of this polar excited state in solvents with higher dielectric constants leads to both red-shifted emission and band broadening, especially visible in DMSO and methanol. The emission profiles in moderate polar solvents (chlorobenzene, THF, chloroform, DMF) are similar in overall shape but differ in peak position and relative intensity. For example, chloroform yields an emission maximum at 500 nm, while THF and chlorobenzene emit slightly blue-shifted to 494 nm. In DMF, the emission peak appears at 504 nm but with reduced intensity and a broader spectral profile compared to less polar media, reflecting enhanced structural relaxation or increased conformational heterogeneity in the excited state. Additionally, the emission spectra in non-polar solvents such as cyclohexane

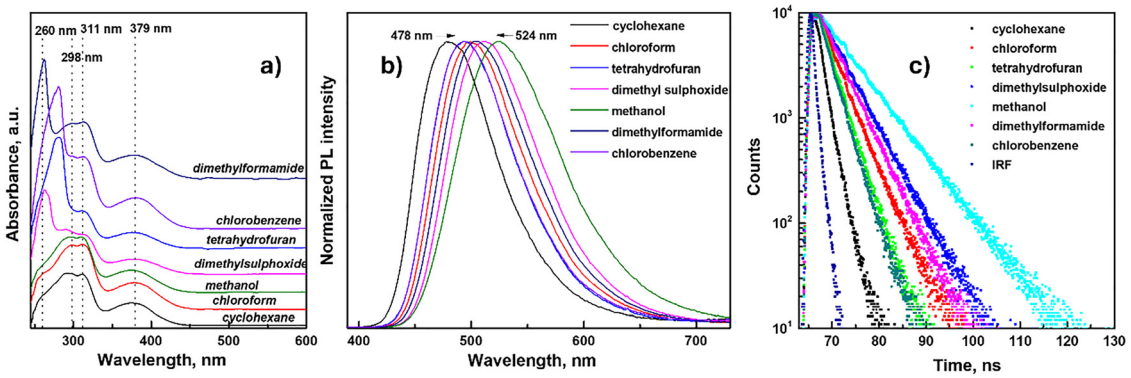


Fig. 2 Solvatochromic behaviour of compound **DMTQ5** in seven solvents of varying polarity: (a) absorption spectra reveal minor solvent-dependent variations in the short-wavelength region; (b) normalized photoluminescence spectra ($\lambda_{exc}$ = 375 nm) display a pronounced bathochromic shift of emission maxima from 528 nm (cyclohexane) to 597 nm (methanol); (c) time-resolved photoluminescence decay curves showing progressive lifetime shortening with decreasing solvent polarity.

and chlorobenzene retain partially resolved vibronic structure, whereas spectral broadening and smoothing in polar solvents point toward increased solvent–solute interactions, reduced rigidity, and enhanced excited-state dipole stabilization. These effects are consistent with solvent-induced reorganization, particularly in flexible, alkyl-substituted D–A–D systems like **DMTQ5**. Overall, the substantial positive solvatochromism observed in emission, in contrast to the weak shifts in absorption, confirms a large dipole moment change between the ground and excited states, reinforcing the donor–acceptor nature of the electronic transitions in **DMTQ5**. These properties render it a promising candidate for polarity-sensitive luminescent probes and functional materials in responsive media.

Time-resolved photoluminescence analysis (TPRL) (Fig. 2(c)) further supports the ICT nature of the emissive state in **DMTQ5**. The decay curves collected across solvents exhibit a clear trend of lifetime shortening with decreasing solvent polarity. In non-polar cyclohexane, **DMTQ5** displays the shortest average decay time ($\tau_{avg} \approx 1.31$ ns), consistent with relatively rigid molecular conformations and reduced nonradiative relaxation channels.[41] Moving to moderately polar solvents such as chloroform, chlorobenzene, and THF, the lifetimes increase to intermediate values ($\tau_{avg} \approx 3.59$–$3.95$ ns), reflecting partial stabilization of the ICT state and enhanced nonradiative pathways. In highly polar media such as DMF, DMSO, and methanol, the excited-state lifetimes become longer ($\tau_{avg} \approx$ 4.86–6.68 ns), accompanied by broader emission bands and lower intensities. This progressive reduction in lifetime highlights the increasing contribution of solvent-induced stabilization and structural relaxation of the polar excited state, which facilitates faster nonradiative deactivation. Taken together with the strong emission solvatochromism, the TRPL results confirm that **DMTQ5** undergoes pronounced solvent-dependent excited-state reorganization. The combination of a relatively rigid conjugated framework with flexible alkyl-substituted fluorene groups allows the molecule to adapt its geometry to the environment, enhancing ICT character in polar solvents.[42] This dual sensitivity, *i.e.*, spectral red shift and lifetime quenching, underscores the potential of **DMTQ5** as a polarity-responsive luminophore and provides mechanistic insight into the balance between radiative and nonradiative decay channels in donor–acceptor–donor chromophores.

### Thermal and electrochemical properties of DMTQ1–DMTQ5

Thermal analysis was performed to assess the thermal stability, melting behaviour, and decomposition characteristics of the synthesized compounds (see SI for more information). All samples exhibited good thermal stability up to approximately 380 °C, with only minimal mass loss (<3%) observed in this range. These initial weight changes are attributed to the evaporation of volatile impurities or residual solvents physically trapped within the matrix. The onset temperatures of decomposition ($T_{onset}$) ranged from 380.6 °C (**DMTQ4**) to 413.2 °C (**DMTQ3**), confirming that the compounds are thermally robust under inert conditions up to this point (Table 2).[7]

DSC analysis revealed distinct melting transitions in three of the five samples (Fig. 3(a) and Fig. S60–S63), with melting onset temperatures ranging from 128.3 °C to 335.6 °C, depending on the molecular structure. Compound **DMTQ5** exhibited several low-temperature endothermic transitions, with peak positions at 129.3, 153.3, and 167.6 °C. These features suggest the presence of polymorphic forms or melting of partially crystalline regions. The main melting event began at approximately 128.3 °C. **DMTQ1** and **DMTQ2** demonstrate well-defined melting transitions at 341.6 °C and 301.3 °C, respectively. This suggests a highly ordered crystalline structure with strong intermolecular interactions. No melting peaks were detected in **DMTQ3** and **DMTQ4**, which may be attributed to the amorphous character.[43]

The decomposition behaviour, as assessed by simultaneous TGA and DTG measurements, varied significantly among the samples, reflecting different degradation mechanisms. Samples **DMTQ1** and **DMTQ2** showed complex multi-step decomposition patterns. In the case of **DMTQ1**, DTG peaks were observed at approximately 457.5, 488.7, 569.7, and 829.7 °C, accompanied by broad endothermic signals on the DSC curve. This suggests sequential fragmentation, likely involving the cleavage of side chains or thermally labile cross-linked units. In contrast, **DMTQ4** and **DMTQ3** underwent rapid, single-step decomposition at temperatures ranging from 416 to 449 °C, with maximum DTG rates of −7.97% $min^{-1}$ and −9.64% $min^{-1}$, respectively. Sharp DTG peaks with high decomposition rates were characteristic of these rapid thermal events, suggesting the presence of energetically unstable structural motifs. Compound **DMTQ5** exhibited intermediate behaviour, with decomposition onset at 386.9 °C and well-resolved DTG maxima at 421.0 °C and 484.2 °C, followed by a broader degradation event at elevated temperatures. Due to the representative nature of its thermal behaviour, the decomposition profile of **DMTQ5** is shown in Fig. 3(a). Complete thermal profiles for all other samples are available in the SI.

The quantitative comparison of TGA data (Fig. 3(b)) revealed substantial differences in thermal resistance and char-forming

Table 2 Characteristic thermal parameters of **DMTQ1–DMTQ5** and mass retention at selected temperatures

| Sample | Initial mass, mg | $T_{onset}$, °C | Mass at 600 °C, % | Residual mass at 1250 °C, % | $T_{p\,max}$ (DTG peak), °C | $T_{melt}$ (DSC), °C |
|---|---|---|---|---|---|---|
| **DMTQ1** | 6.49 | 410.4 | 85.02 | 72.33 | 488.7 | 335.6 |
| **DMTQ2** | 5.35 | 402.6 | 81.60 | 68.36 | 517.8 | 301.3 |
| **DMTQ3** | 6.45 | 413.2 | 42.18 | 34.62 | 446.8 | — |
| **DMTQ4** | 4.71 | 380.6 | 44.91 | 31.95 | 416.3 | — |
| **DMTQ5** | 6.30 | 386.9 | 58.52 | 48.78 | 421.0 | 128.3 |

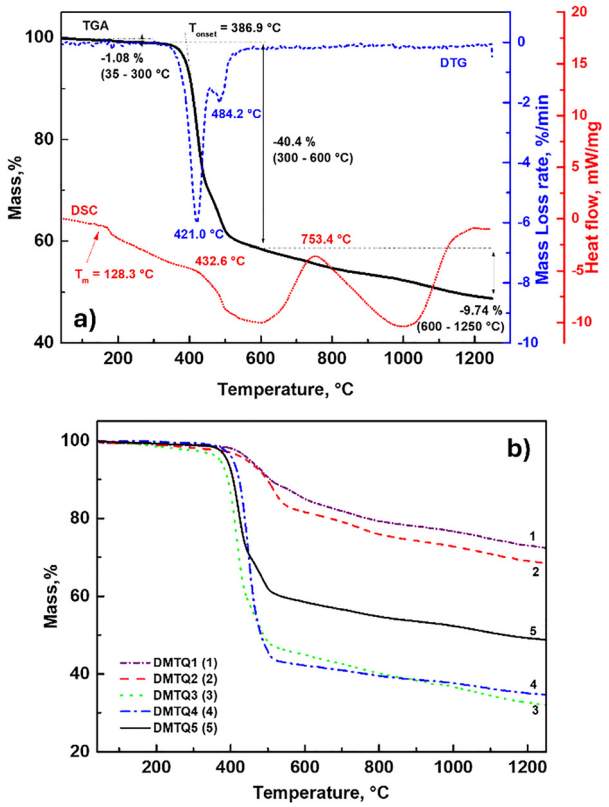


Fig. 3 (a) Combined thermogravimetric (TGA, black solid), derivative thermogravimetric (DTG, blue dashed), and differential scanning calorimetry (DSC, red dotted) profiles of sample **DMTQ5**, measured simultaneously under nitrogen atmosphere (50 ml $min^{-1}$) at a heating rate of 10 °C $min^{-1}$. The graph also indicates the evaluated parameters, including mass changes, $T_{onset}$, melting temperature, and the peak maxima of DTG and DSC signals associated with the observed decomposition. (b) Comparison of thermogravimetric (TGA) curves for all synthesized compounds **DMTQ1–DMTQ5** measured under nitrogen atmosphere.

tendencies. **DMTQ1** exhibited the highest stability, with 85.02% mass retention at 600 °C and 72.33% residual mass at 1250 °C, indicating significant carbonization or the presence of thermally stable inorganic content. In contrast, **DMTQ4** was the least stable, retaining only 44.91% at 600 °C and dropping to 31.95% at 1250 °C, consistent with extensive volatilization and limited residue formation. Above 600 °C, **DMTQ1** underwent the smallest additional mass loss (*ca.* 13%), while **DMTQ4** showed a further 13% reduction, suggesting higher volatility and less efficient char formation. Taken together, the thermal profiles provide insight into the intrinsic stability of the materials, influenced by molecular architecture, the presence of inorganic residues, and differences in char-forming capabilities.

Cyclic voltammetry (CV) measurements were performed to evaluate the frontier orbital energies of the **DMTQ** series (Fig. 4). Experiments were conducted in DMF with 0.1 M $TBAPF_6$ at a scan rate of 50 mV $s^{-1}$ using a Platinum working electrode, a Platinum counter electrode, and Ag/AgCl as the reference electrode. All potentials were referenced to the $Fc/Fc^+$ couple. All five compounds exhibit clear oxidation processes

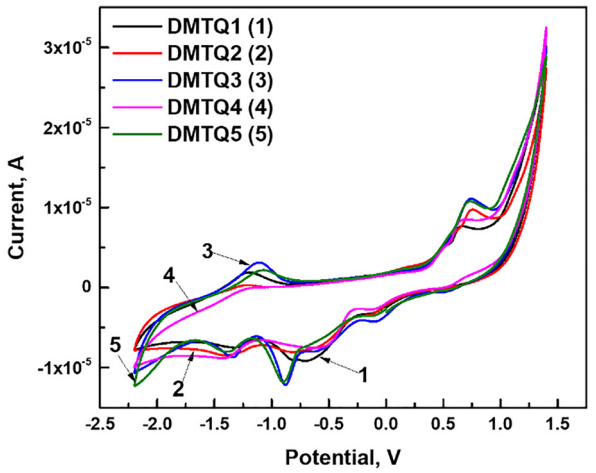


Fig. 4 Cyclic voltammograms of **DMTQ1–DMTQ5** recorded in DMF containing 0.1 M $TBAPF_6$ at a scan rate of 50 mV $s^{-1}$ using a Pt working electrode, Pt counter electrode, and Ag/AgCl reference electrode.

with onsets ranging from 0.54 to 0.64 V (Table 1).[44] The onset potentials were determined by the intersection of the tangent to the rising current with the baseline. The corresponding HOMO levels were calculated using the relation: $E_{HOMO} = -(E_{ox,onset} + 4.80)$ eV, giving values from −5.34 eV (**DMTQ4**) to −5.44 eV (**DMTQ2**). The narrow dispersion of HOMO energies ($\Delta \approx 0.10$ eV) indicates that all derivatives share a similar oxidation profile, with subtle differences arising from the steric and electronic character of the 9,9-substituents on the fluorene units. Among the series, **DMTQ2** exhibits the deepest HOMO level (−5.44 eV), which is consistent with its slightly higher oxidation onset potential (0.64 V) and blue-shifted emission maximum (487 nm). Within the scanned potential window, no reduction processes were observed up to −2.0 V, confirming that the LUMO is localized predominantly on the electron-deficient quinoxaline core.

LUMO energies were therefore derived from the optical band gap according to: $E_{LUMO} = E_{HOMO} + E_g$, $E_g = 1240/\lambda_{onset(ABS)}$.[45] The resulting LUMO energy levels fall within −2.57 to −2.67 eV, showing negligible variation across the series. The electrochemical band gaps (≈2.77 eV) are in excellent agreement with the optical gaps extracted from absorption edges, further supporting the donor–acceptor–donor (D–A–D) architecture of these chromophores.

The electrochemical measurements revealed small variations in the HOMO energy levels (from −5.34 to −5.44 eV) and LUMO energy levels (from −2.57 to −2.67 eV) across the **DMTQ** series. These subtle shifts suggest that the substituents at the 9,9-position of fluorene have a slight influence on the donor strength and local conformation, while the quinoxaline–thiophene core, which determines the LUMO, remains largely unaffected. As a result, the HOMO–LUMO gaps and the corresponding optical band gaps are nearly constant for all derivatives.

Taken together, the CV data highlight the modular effect of fluorene substitution at the 9,9-position: while the electron-accepting

quinoxaline core defines a nearly invariant LUMO, steric and electronic tuning of the donor blocks leads to subtle yet measurable differences in HOMO levels. This electronic structure accounts for the consistent photophysical phenomena observed across **DMTQ1–DMTQ5**, with emission maxima ranging from 490 to 502 nm, quantum yields of up to 45%, and excited-state lifetimes of 2.7–4.0 ns.

Although no DFT calculations were performed in this study, the experimental data provide a consistent picture of the electronic structure of the **DMTQ** derivatives. The nearly identical absorption onsets and optical band gaps (Table 1) together with the electrochemical HOMO–LUMO levels suggest that the LUMO is mainly localized on the quinoxaline–thiophene acceptor core, while the HOMO is distributed over the fluorene donor fragments. This interpretation aligns well with previously reported DFT results for structurally related quinoxaline systems,[46–48] confirming that the variation in the 9,9-substituents predominantly affects the HOMO energy and molecular conformation, rather than the overall electronic coupling.

### Solid-state emission and light-responsive behaviour

Despite the structural resemblance of the synthesized compounds to diarylethenes,[49] well known for their photochromic switching, none of the **DMTQ** derivatives exhibited noticeable photoresponsive features in dilute chloroform solution under UV irradiation. This initial observation suggested that in solution, the excited-state behaviour remains relatively simple and is dominated by monomeric fluorescence. To evaluate the potential of these materials for optoelectronic applications, we investigated their photophysical behaviour in the solid state, focusing on neat thin films and films embedded in PMMA. Unexpectedly, both the films and drop-cast LED coatings of **DMTQ2** and **DMTQ4** demonstrate pronounced solid-state emission with a strong bathochromic shift relative to the solution phase, accompanied by vivid and distinguishable fluorescence colours under UV light (Fig. 5). Moreover, a clear light-induced response, including a reversible change in emission intensity and colour, was observed as an emergent photoresponsive property absent in the solution state.[50]

Fig. 5(a) presents the excitation and emission spectra of **DMTQ2** in neat and PMMA-embedded films.

The emission maximum undergoes a red shift of more than 100 nm compared to the solution (from ~480 nm in chloroform to ~620 nm in neat film), and the emission in the neat film appears relatively narrow and intense. In contrast, the PMMA film exhibits a broader profile with an additional high-energy shoulder at around 480 nm, which closely matches the emission observed in the chloroform solution. The pronounced red shift observed in the neat film is associated with light-induced structural reorganization, characteristic of the photochromic nature of this compound. In solution, solvation by chloroform stabilizes the molecular configuration and significantly slows down this transformation. In the neat film, where solvent effects are absent, the molecules can undergo the photoinduced rearrangement much more readily, leading to a lower-energy emissive state and a distinct, red-shifted emission. In contrast, when dispersed in the PMMA matrix, the polymer environment further limits and retards such photo-induced changes, so the emission retains also the spectral features of the unconverted form. The excitation spectrum in the solid-state reveals enhanced low-energy features, possibly

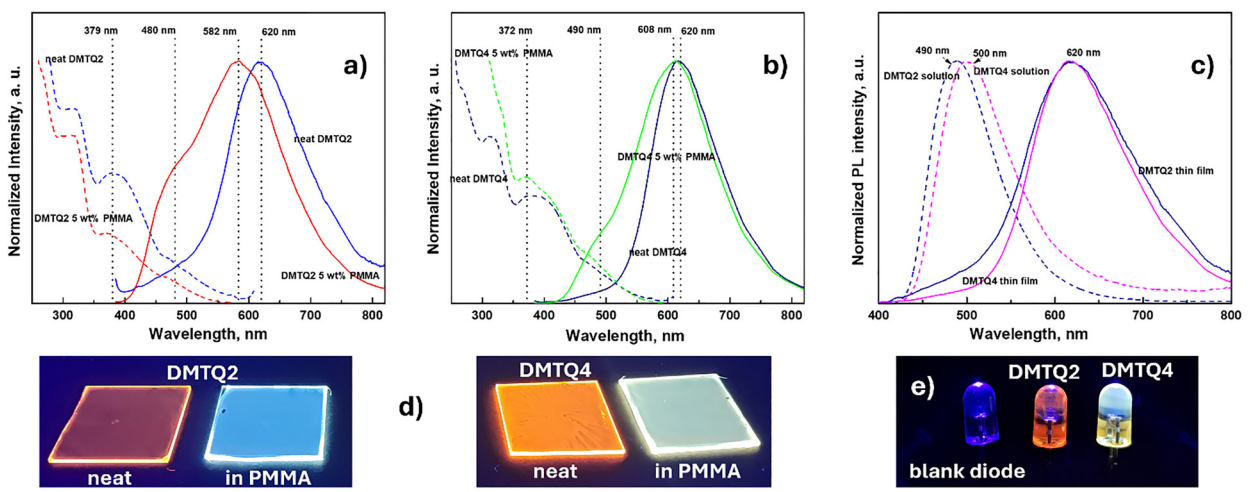


Fig. 5 Photophysical and photoresponsive properties of compounds DMTQ2 and DMTQ4 in the solid state. (a) Normalized excitation (dashed lines) and emission (solid lines) spectra of DMTQ2 in neat film (red) and in PMMA matrix (blue); (b) same for DMTQ4 in neat film (green) and in PMMA (dark blue); (c) comparison of excitation and emission spectra of DMTQ2 (blue) and DMTQ4 (magenta) in chloroform and in neat films. In all cases, a pronounced bathochromic shift and broadening of the emission band are observed upon transitioning from solution to solid state. (d) Photographs of thin films of DMTQ2 (right) and DMTQ4 (left) (neat and in PMMA) under UV light (365 nm), highlighting bright fluorescence with distinct colour contrast. (e) Fluorescence of UV-LEDs coated with DMTQ2 and DMTQ4 in polymer matrix (in comparison to blank diode), demonstrating solid-state light responsiveness absent in solution.

associated with π–π stacking or conformational planarization in the aggregated state. Fig. 5(b) shows similar measurements for **DMTQ4**, which features branched alkyl substituents on the fluorene core. While this substitution reduces aggregation compared to **DMTQ2**, **DMTQ4** still demonstrates a substantial bathochromic shift in the neat film (∼580 nm) and retains a red-emissive character in PMMA. Notably, both materials maintain good fluorescence intensity in polymer matrices, which is advantageous for practical implementation. Fig. 5(c) compares the normalized emission and excitation spectra of **DMTQ2** and **DMTQ4** in solution and solid state. While both compounds exhibit a strong red shift upon solidification, **DMTQ4** shows a nearly complete overlap of the emission maxima in neat and PMMA films, in contrast to **DMTQ2**, which displays a more pronounced spectral separation. In both cases, a high-energy shoulder is visible in PMMA films, likely due to emission from isolated or weakly interacting species. These differences suggest that the more rigid and planar structure of **DMTQ2** leads to stronger aggregation effects and less compatibility with the polymer matrix, whereas the branched and flexible substituents in **DMTQ4** promote better dispersion and spectral uniformity across media. This highlights the critical role of molecular packing and environment in modulating emissive behaviour. Fig. 5(c) and (d) visually confirm the striking colour differences in solid-state emission. Under UV illumination, **DMTQ2** and **DMTQ4** films emit intense red and yellow fluorescence, respectively, while their PMMA films revert to cooler blue tones.[51] Moreover, when coated onto standard UV-LED diodes, both compounds display well-defined red luminescence, underscoring their utility as emissive materials with stimulus-dependent behaviour.

These findings are of particular interest from both fundamental and applied perspectives. The emergence of light-induced emissive switching exclusively in the solid state highlights a potentially novel class of materials exhibiting solid-state-specific photochromism. This warrants further investigation into the underlying mechanisms, such as conformational changes, aggregation effects, or excited-state reorganization, and their tunability through molecular design. In addition to their photonic relevance, such compounds may offer valuable functionality for optoelectronic devices, including light-responsive coatings, information storage systems, and wavelength-tunable emitters. Given their strong absorption, good film-forming ability, and red emission, these materials may also be promising candidates for active layers in solar cells or luminescent solar concentrators.

## Conclusions

In this work, we synthesized and comprehensively characterized a new series of quinoxaline-based D–A–D emitters (**DMTQ1–DMTQ5**), combining electron-rich 2,5-dimethylthiophene donors with fluorene units bearing diverse 9,9-substituents. The modular design enables the predictable tuning of photophysical and electrochemical properties while maintaining a common quinoxaline-centred acceptor. In solution, all derivatives display broad ICT-type emission with solvent-dependent shifts, and **DMTQ5** in particular demonstrates pronounced solvatochromism and polarity-dependent excited-state lifetimes. Electrochemical measurements revealed narrow variations in HOMO levels (−5.34 to −5.44 eV) governed by fluorene substitution, while LUMO energies remained largely anchored to the quinoxaline core, yielding band gaps in good agreement with optical data (∼2.8 eV). Importantly, spin-coated films of selected derivatives exhibit reversible photochromic emission switching under UV irradiation, a feature not observed in solution and easily demonstrated on a UV-LED platform. These findings underscore the importance of fluorene substitution as a powerful tool for tailoring both molecular and film-state emissive behaviour, opening up opportunities for applications in OLED-relevant layers, visual indicators, and light-responsive materials.

## Author contributions

Liudmila Loghina: writing – original draft, supervision, methodology, investigation, formal analysis, data curation, and conceptualization. Jiri Jancalek, Jakub Houdek, Zuzana Zmrhalova, Roman Jambor, Miroslav Vlcek: formal analysis, data curation, visualization, and writing – review and editing. Roman Jambor, Miroslav Vlcek: supervision and project administration.

## Conflicts of interest

There are no conflicts to declare.

## Data availability

The datasets generated and analyzed during the current study – including FTIR, UV-Vis, PL, and TGA data – are available in the Figshare repository: **https://doi.org/10.6084/m9.figshare.29858648**.

Supplementary information (SI): synthesis methods, characterization methods, TGA data, $^{1}H$, $^{13}C$ NMR, and FTIR spectra of the synthesized compounds. See DOI: **https://doi.org/10.1039/d5ma01158b**.

## Acknowledgements

Authors appreciate the financial support from the project ''Innovative materials with high added value suitable for applications – INMA'' (CZ.02.01.01/00/23_021/0008593), support from the grant LM2023037 from the Ministry of Education, Youth and Sports of the Czech Republic.

## Notes and references


1 S. B. Mdluli, M. E. Ramoroka, S. T. Yussuf, K. D. Modibane, V. S. John-Denk and E. I. Iwuoha, *Polymers*, 2022, **14**(4), 716, DOI: 10.3390/polym14040716.

2 A. G. S. Al-Azzawi, S. B. Aziz, E. M. A. Dannoun, A. Iraqi, M. M. Nofal, A. R. Murad and A. M. Hussein, *Polymers*, 2023, **15**(1), 164, DOI: 10.3390/polym15010164.

3 F. Ullah, K. Hasrat, S. Iqbal and S. Wang, *Molecules*, 2024, **29**(22), 5369, DOI: 10.3390/molecules29225369.

4 D. Cappello, F. L. Buguis and J. B. Gilroy, *ACS Omega*, 2022, **7**(36), 32727, DOI: 10.1021/acsomega.2c04401.

5 Y. Takeda, *Acc. Chem. Res.*, 2024, **57**(15), 2219, DOI: 10.1021/acs.accounts.4c00353.

6 S. Izumi, H. F. Higginbotham, A. Nyga, P. Stachelek, N. Tohnai, P. de Silva, P. Data, Y. Takeda and S. Minakata, *J. Am. Chem. Soc.*, 2020, **142**(3), 1482, DOI: 10.1021/jacs.9b11578.

7 M. Sigl, T. Rath, B. Schlemmer, P. Fürk and G. Trimmel, *Monatsh. Chem.*, 2023, **154**, 543, DOI: 10.1007/s00706-022-03030-7.

8 E. J. Lee and H. J. Song, *Polymers*, 2020, **12**(12), 2859, DOI: 10.3390/polym12122859.

9 W. Zhuang, A. Lundin and M. R. Andersson, *J. Mater. Chem. A*, 2014, **2**, 2202, DOI: 10.1039/C3TA14456A.

10 Y. Li, H. Tong, Z. Xie and L. Wang, *Polym. Chem.*, 2013, **4**, 2884, DOI: 10.1039/C3PY00148B.

11 X. Li, Y. Chen, S. Li, A. Li, L. Tu, D. Zhang, L. Duan, Y. Xie, B. Z. Tang and Z. Li, *J. Mater. Chem. C*, 2023, **11**, 5217, DOI: 10.1039/D2TC04403J.

12 L. Yu, Z. Wu, G. Xie, C. Zhong, Z. Zhu, D. Ma and C. Yang, *Chem. Commun.*, 2018, **54**, 1379, DOI: 10.1039/C7CC09925H.

13 J. H. Kim, C. E. Song, H. U. Kim, I. N. Kang, W. S. Shin, M. J. Park and D. H. Hwang, *J. Polym. Sci., Part A: Polym. Chem.*, 2013, **51**, 4136, DOI: 10.1002/pola.26823.

14 K. Zhao, W. Wang, C. Kang, Z. Zhang, H. Xu, Q. Liu and H. Dai, *J. Mater. Chem. C*, 2025, **13**, 12005, DOI: 10.1039/D5TC01087J.

15 J. Zhang, W. Cai, F. Huang, E. Wang, C. Zhong, S. Liu, M. Wang, C. Duan, T. Yang and Y. Cao, *Macromolecules*, 2011, **44**(4), 894, DOI: 10.1021/ma1027164.

16 wJ. Wu, G. Lai, Z. Li, Y. Lu, T. Leng, Y. Shen and C. Wang, *Dyes Pigm.*, 2016, **124**, 268, DOI: 10.1016/j.dyepig.2015.09.021.

17 L. K. Wang, J. J. Zhou, Y. B. Lan, S. Y. Ding, W. Yu and W. Wang, *Angew. Chem., Int. Ed.*, 2019, **58**(28), 9443, DOI: 10.1002/anie.201903534.

18 L. I. Belen'kii, V. Z. Shirinyan, G. P. Gromova, A. V. Kolotaev, Y. A. Strelenko, S. N. Tandura, A. N. Shumskii and M. M. Krayushkin, *Chem. Heterocycl. Compd.*, 2003, **39**, 1570, DOI: 10.1023/B:COHC.0000018333.96922.68.

19 M. Caliskan, M. C. Erer, S. T. Aslan, Y. A. Udum, L. Toppare and A. Cirpan, *Dyes Pigm.*, 2020, **180**, 108479, DOI: 10.1016/j.dyepig.2020.108479.

20 G. Marotta, Ch. P. Kumar, M. G. Lobello, F. Cavazzini, P. Salvatori, K. Ganesh, M. K. Nazeeruddin, M. Chandrasekharam and F. De Angelis, *Dalton Trans.*, 2015, **44**, 5369, DOI: 10.1039/C4DT03633F.

21 X. Song, Y. Zhang, Y. Li, F. Li, X. Bao, D. Ding, M. Sun and R. Yang, *Macromolecules*, 2017, **50**(17), 6880, DOI: 10.1021/acs.macromol.7b00998.

22 L. Lyu, R. Su, S. Y. Al-Qaradawi, K. A. Al-Saad and A. El-Shafei, *Dyes Pigm.*, 2019, **171**, 107683, DOI: 10.1016/j.dyepig.2019.107683.

23 N. Schäfer, L. Glanz, A. Lützen and F. Beuerle, *Org. Chem. Front.*, 2025, **12**, 1763, DOI: 10.1039/D4QO02012J.

24 J. Jo, C. Chi, S. Hoger, G. Wegner and D. Y. Yoon, *Chem. – Eur. J.*, 2004, **10**, 2681, DOI: 10.1002/chem.200305659.

25 Y. Jiang, K. F. Li, K. Gao, H. Lin, H. L. Tam, Y. Y. Liu, Y. Shu, K. L. Wong, W. Y. Lai, K. W. Cheah and W. Huang, *Angew. Chem., Int. Ed.*, 2021, **60**, 10007, DOI: 10.1002/anie.202100542.

26 B. M. Lucht, R. J. Monsky, M. C. Rosko, J. M. Tanski and J. M. Nadeau, *Tetrahedron*, 2025, **170**, 134382, DOI: 10.1016/j.tet.2024.134382.

27 A. P. Kulkarni, Y. Zhu and S. A. Jenekhe, *Macromolecules*, 2005, **38**(5), 1553, DOI: 10.1021/ma048118d.

28 Z. Barbierikova, D. Dvoranova, M. Bella, V. Milata, A. Czimerova and V. Brezova, *Molecules*, 2014, **19**(8), 12078, DOI: 10.3390/molecules190812078.

29 D. Gedefaw, M. Prosa, M. Bolognesi, M. Seri and M. R. Andersson, *Adv. Energy Mater.*, 2017, **7**, 1700575, DOI: 10.1002/aenm.201700575.

30 P. Ledwon, R. Motyka, K. Ivaniuk, A. Pidluzhna, N. Martyniuk, P. Stakhira, G. Baryshnikov, B. F. Minaev and H. Agren, *Dyes Pigm.*, 2020, **173**, 108008, DOI: 10.1016/j.dyepig.2019.108008.

31 T. G. Mayerhöfer, A. V. Pipa and J. Popp, *ChemPhysChem*, 2019, **20**, 2748, DOI: 10.1002/cphc.201900787.

32 M. M. Xue, Y. M. Xie, L. S. Cui, X. Y. Liu, X. D. Yuan, Y. X. Li, Z. Q. Jiang and L. S. Liao, *Chem. – Eur. J.*, 2016, **22**, 916, DOI: 10.1002/chem.201503041.

33 L. Bai, B. Liu, Y. Han, M. Yu, J. Wang, X. Zhang, C. Ou, J. Lin, W. Zhu, L. Xie, C. Yin, J. Zhao, J. Wang, D. D. C. Bradley and W. Huang, *ACS Appl. Mater. Interfaces*, 2017, **9**(43), 37856, DOI: 10.1021/acsami.7b08980.

34 J. W. Eastman, *Photochem. Photobiol.*, 1967, **6**, 55, DOI: 10.1111/j.1751-1097.1967.tb08790.x.

35 J. Dai and X. Zhang, *Chem. Biomed. Imaging*, 2023, **1**(9), 796, DOI: 10.1021/cbmi.3c00091.

36 Q. Gu, F. Chotard, J. Eng, A. P. M. Reponen, I. J. Vitorica-Yrezabal, A. W. Woodward, T. J. Penfold, D. Credgington, M. Bochmann and A. S. Romanov, *Chem. Mater.*, 2022, **34**(16), 7526, DOI: 10.1021/acs.chemmater.2c01938.

37 E. V. Verbitskiy, P. le Poul, F. Bures, S. Achelle, A. Barsella, Y. A. Kvashnin, G. L. Rusinov and V. N. Charushin, *Molecules*, 2022, **27**(13), 4250, DOI: 10.3390/molecules27134250.

38 I. Aburto, M. Vidal, S. Yanez, C. Aliaga and M. Dominguez, *Dyes Pigm.*, 2025, **233**, 112489, DOI: 10.1016/j.dyepig.2024.112489.

39 W. Kanezaki, R. Ishikawa and H. Tsuji, *Eur. J. Org. Chem.*, 2025, e202401471, DOI: 10.1002/ejoc.202401471.

40 G. H. Pujar, N. Deshapande, I. A. M. Khazi and S. R. Inamdar, *J. Mol. Liq.*, 2018, **271**, 118, DOI: 10.1016/j.molliq.2018.08.107.

41 H. Zhu, M. Li, J. Hu, X. Wang, J. Jie, Q. Guo, C. Chen and A. Xia, *Sci. Rep.*, 2016, **6**, 24313, DOI: 10.1038/srep24313.

42 J. Cerezo, S. Gao, N. Armaroli, F. Ingrosso, G. Prampolini, F. Santoro, B. Ventura and M. Pastore, *Molecules*, 2023, **28**(9), 3910, DOI: **10.3390/molecules28093910**.
43 G. Lewinska, K. Khachatryan, K. S. Danel, Z. Danel, J. Sanetra and K. W. Marszalek, *Polymers*, 2020, **12**(11), 2707, DOI: **10.3390/polym12112707**.
44 C. M. Cardona, W. Li, A. E. Kaifer, D. Stockdale and G. C. Bazan, *Adv. Mater.*, 2011, **23**, 2367, DOI: **10.1002/adma.201004554**.
45 M. A. Pan, T. K. Lau, Y. Tang, Y. C. Wu, T. Liu, K. Li, M. C. Chen, X. Lu, W. Ma and C. Zhan, *J. Mater. Chem. A*, 2019, **7**, 20713, DOI: **10.1039/C9TA06929A**.
46 Y. He, S. Yagi, T. Maeda and H. Nakazumi, *Mol. Cryst. Liq. Cryst.*, 2015, **621**(1), 64, DOI: **10.1080/15421406.2015.1095927**.
47 L. Bhattacharya, A. Brown, S. Sharma and S. Sahu, *J. Phys. Chem. A*, 2022, **126**(40), 7110, DOI: **10.1021/acs.jpca.2c03906**.
48 S. Fagour, D. Thirion, A. Vacher, X. Sallenave, G. Sini, P.-H. Aubert, F. Vidala and C. Chevrot, *RSC Adv.*, 2017, **7**, 22311, DOI: **10.1039/C7RA02535A**.
49 M. Irie, T. Fukaminato, K. Matsuda and S. Kobatake, *Chem. Rev.*, 2014, **114**(24), 12174, DOI: **10.1021/cr500249p**.
50 M. Irie, *Chem. Rev.*, 2000, **100**(5), 1683, DOI: **10.1021/cr980068l**.
51 R. A. Evans, T. L. Hanley, M. A. Skidmore, T. P. Davis, G. K. Such, L. H. Yee, G. E. Ball and D. A. Lewis, *Nat. Mater.*, 2005, **4**, 249, DOI: **10.1038/nmat1326**.